HHS Public Access

Author manuscript

Nat Methods. Author manuscript; available in PMC 2020 March 31.

Published in final edited form as:

Nat Methods. 2019 January ; 16(1): 95–102. doi:10.1038/s41592-018-0232-7.

A pH-correctable, DNA-based fluorescent reporter for organellar Calcium

Nagarjun Narayanaswamy[#,1,2], **Kasturi Chakraborty**[#,1,2,*], **Anand Saminathan**[1,2], **Elizabeth Zeichner**[1], **KaHo Leung**[1,2], **John Devany**[3], **Yamuna Krishnan**[1,2,*]

[1]Department of Chemistry, The University of Chicago, Chicago, Illinois 60637, USA.

[2]Grossman Institute of Neuroscience, Quantitative Biology and Human Behavior, The University of Chicago, Chicago, Illinois 60637, USA.

[3]Department of Physics, The University of Chicago, IL, 60637, USA

Abstract

It is extremely challenging to quantitate lumenal Ca^{2+} in acidic Ca^{2+} stores of the cell because all Ca^{2+} indicators are pH sensitive, and Ca^{2+} transport coupled to pH in acidic organelles. We have developed a fluorescent DNA-based reporter, *CalipHluor*, that is targetable to specific organelles. By ratiometrically reporting lumenal pH and Ca^{2+} simultaneously, it functions as a pH-correctable, Ca^{2+} reporter. By targeting *CalipHluor* to the endolysosomal pathway we mapped lumenal Ca^{2+} changes during endosomal maturation and found a surge in lumenal Ca^{2+} specifically in lysosomes. Using lysosomal proteomics and genetic analysis we found that *catp-6*, a *C. elegans* homolog of ATP13A2, was responsible for lysosomal Ca^{2+} accumulation - the first example of a lysosome-specific Ca^{2+} importer in animals. By enabling the facile quantification of compartmentalized Ca^{2+}, *CalipHluor* can expand our understanding of subcellular Ca^{2+} importers.

Introduction

Ca^{2+} regulates diverse cellular functions upon its controlled release from different intracellular stores that initiates signaling cascadeszz[1,2]. Lysosomes have recently been recognized as “acidic Ca^{2+} stores”, and lumenal Ca^{2+} is central to its diverse functions[3]. Lysosome function is particularly important in neurons given the preponderance of lysosome-related genes in diverse neurological disorders including ~60 lysosomal storage disorders[4]. For example, risk genes for Parkinsons disease such as LRRK2, ATP6AP2, ATP13A2, and genetic risk associated GBA1 gene, are predicted to act in lysosomal pathways[5].

[*]Corresponding authors. yamuna@uchicago.edu; kasturi@uchicago.edu.
[#]These authors contributed equally to this work.

Author Contributions

K.C. and Y.K. designed the project. N.N synthesized and designed the calcium dye. N.N., K.C., A.S., E.H.Z., K.L., performed experiments. J.D. provided key resources. N.N., K.C., A.S, and Y.K. analyzed the data. K.C. and Y.K wrote the paper. All authors discussed the results and gave inputs on the manuscript.

Competing financial interests

The authors declare no competing financial interests.

Although electrophysiology has enabled the discovery of several channels that release lysosomal Ca^{2+}, mediators of lysosomal Ca^{2+} import have not yet been identified[3,6]. Lysosomal Ca^{2+} release channels are amenable to investigation because Ca^{2+} release can be tracked using cytosolic Ca^{2+} dyes or genetically encoded Ca^{2+} indicators anchored to the cytoplasmic face of the lysosome[7–9]. Upon Ca^{2+} release, these probes indicate cytosolic Ca^{2+} in the area surrounding lysosomes. In contrast, lumenal Ca^{2+} cannot be quantitated, impeding the study of lysosomal Ca^{2+} importers. Consequently, lysosomal Ca^{2+} importers have not yet been identified in animals[10], with the closest evidence being that the *Xenopus* CAX gene localizes in lysosomes upon overexpression[11].

The inability to quantify Ca^{2+} in acidic organelles arises because all Ca^{2+} indicators function by coordinating Ca^{2+} through carboxylate groups that get protonated at acidic pH[12]. This changes probe affinity to Ca^{2+} ions. Further, organellar pH is coupled to lumenal Ca^{2+} entry and exit[13]. Thus, it is non-trivial to deconvolute the contribution of Ca^{2+} to the observed fluorescence changes of any Ca^{2+} indicator. Previous attempts used endocytic tracers bearing either pH or Ca^{2+} sensitive dyes to serially measure population-averaged pH and apparent Ca^{2+} in different batches of cells thus, scrambling information from individual endosomes [13–17]. Given the broad pH distribution in endocytic organelles, this approach does not provide the resolution needed to study Ca^{2+} import[18].

Here, we use a combination reporter for pH and Ca^{2+} to map both ions in parallel in the same endosome with single endosome addressability, achieving highly accurate measures of lumenal Ca^{2+}. Using the pH reporter module of the combination reporter we deduce the pH in individual endosomes. By knowing exactly how the affinity of the Ca^{2+} sensitive module, i.e., its dissociation constant, K_d, changes with pH, we apply a K_d correction factor suited to the lumenal pH of each endosome to thereby compute the true value of lumenal Ca^{2+} with single-endosome resolution.

DNA nanodevices are versatile chemical reporters that can quantitatively map second messengers in real time, in living systems[19–22]. The modularity of DNA allows us to integrate distinct functions in precise stoichiometries into a single assembly. These include (i) a module to fluorescently sense a given ion (ii) a normalizing module for ratiometric quantitation and (iii) a targeting module to localize the reporter in a specific organelle[19]. We have thus measured H^+ and Cl^- in endocytic organelles[20–24]. Here we describe a DNA-based fluorescent reporter, *CalipHluor*, to quantitatively map organellar pH and Ca^{2+} simultaneously and with single organelle addressability. *CalipHluor* comprises four modules: a pH sensitive module; a Ca^{2+} sensitive fluorophore; an internal reference dye to ratiometrically quantitate pH as well as Ca^{2+} and finally, a targeting domain to transport *CalipHluor* to a specific organelle.

By targeting *CalipHluor* to the scavenger receptor-mediated endocytic pathway, we mapped lumenal Ca^{2+} as a function of endosomal maturation in nematodes. We found that Ca^{2+} is fairly low in early and late endosomes, followed by a ~35 fold surge in lumenal Ca^{2+} in lysosomes - implicating the existence of lysosome-specific Ca^{2+} import mechanisms. We identified the P5 Ca^{2+}ATPase ATP13A2 as a potential candidate given its similarity to a well-known Ca^{2+} importer in the endoplasmic reticulum[25]. ATP13A2 transports divalent

ions such as Mg^{2+}, Mn^{2+}, Cd^{2+}, Zn^{2+} yet, has not been tested for its ability to transport Ca^{2+}[26,27]. We showed that the *C. elegans* homolog of ATP13A2, *catp-6*, functions in opposition to the well-known lysosomal Ca^{2+} release channel, *cup-5* [28]. We then showed that the human homolog, ATP13A2 also facilitates lysosomal Ca^{2+} entry by measuring lysosomal Ca^{2+} in fibroblasts derived from patients with Kufor Rakeb Syndrome. This constitutes the first example of a lysosomal Ca^{2+} importer in the animal kingdom.

Results and Discussion

Design and *in vitro* characterization of *CalipHluor*

We describe the design and characterization of a fluorescent, DNA-based combination reporter for pH and Ca^{2+} called $CalipHluor_{Ly}$. $CalipHluor_{Ly}$ is a 57-base pair DNA duplex comprising two strands D1 and D2 and bears three distinct domains (Fig. 1a, Supplementary Table S1). The first domain in $CalipHluor_{Ly}$ is a Ca^{2+}-reporter domain that uses a novel small molecule that functions as a Ca^{2+} indicator that we denote Rhod-5F[29]. Rhod-5F consists of a BAPTA core, a rhodamine fluorophore (λ_{ex} = 560 nm; λ_{em} = 580 nm) and an azide linker. In the absence of Ca^{2+}, the rhodamine fluorophore in Rhod-5F is quenched by photoinduced electron transfer (PeT) from the BAPTA core. Upon Ca^{2+} chelation quenching is relieved resulting in high fluorescence. Note that protonation of the amines in BAPTA also relieves PeT[12]. Thus the percentage change in signal as well as the dissociation constant (K_d) in Rhod-5F will be affected as a function of pH. The K_d of Rhod-5F for Ca^{2+} binding is indeed pH dependent and shown in the supplementary information (Supplementary Fig. S1).

Rhod-5F is attached to the D2 strand bearing a dibenzocyclooctyne (DBCO) group using click chemistry [30]. Conjugation to D2 did not change the K_d of Rhod-5F in $CalipHluor_{Ly}$ (Fig. 1b). In $CalipHluor_{Ly}$ Rhod-5F (O, orange diamond) shows a K_d of 1.1 μM at pH 7.2 which increases as acidity increases (Fig. 1b).

For ratiometric quantification of Ca^{2+} we incorporate Alexa 647 as a reference dye (λ_{ex} = 630 nm; λ_{em} = 665 nm) on $CalipHluor_{Ly}$ positioned so that it does not FRET with Rhod-5F. Alexa 647 was chosen for its negligible spectral overlap with Rhod-5F and insensitivity to pH, Ca^{2+} and other ions (red circle, Fig. 1a). The fixed stoichiometry of Alexa 647 efficiently corrects for Rhod-5F intensity changes due to inhomogeneous probe distribution in cells, thus making the ratio of Rhod-5F (O) and Alexa 647 (R) intensities in *CalipHluor* probes proportional to pH and Ca^{2+}. The second domain (gray line) constitutes a DNA based pH-reporter domain that we have previously described, called the *I-switch*[20] (Fig. 1a). This *I-switch* has been used to map pH in diverse endocytic organelles in living cells[20–24]. To map pH in early and late endosomes we made *CalipHluor*, a variant suited to the lower acidities in these organelles (Supplementary Table S1 and Fig. S2c). *CalipHluor* and $CalipHluor_{Ly}$ were formed and characterized by gel electrophoresis (Supplementary Fig. S2 a–e). The third ‘integration’ domain comprises a 30-mer duplex, that integrates the pH and the Ca^{2+} reporter domains into a single DNA assembly. One end is fused to the *I-switch* and the other is fused to the Ca^{2+} sensor. This domain also helps in targeting, because its anionic nature aids recognition and trafficking by scavenger receptors in a DNA sequence independent manner [21].

The response characteristics of *CalipHluor* and *CalipHluor*$_{Ly}$ were investigated as a function of pH as well as Ca^{2+} and their pH and Ca^{2+} sensitive regimes were determined (Fig. 1c–d and Supplementary Fig. S2f–g). A 3D surface plot of D/A as a function of pH and different values of free [Ca^{2+}] is shown in Fig. 1c. These revealed that the pH reporting capabilities of *CalipHluor* and *CalipHluor*$_{Ly}$ are between pH 5.0 – 7.0 and pH 4.0 – 6.5 with fold changes in D/A ratios of 4.0 and 5.5 respectively (Fig. 1c)[21]. Notably, the fold changes in D/A ratios were invariant over a range of free Ca^{2+} concentrations from 20 nM – 10 mM showing that pH sensing by these probes is unaffected by Ca^{2+} levels (Fig. 1c).

In parallel, the intensities of Rhod-5F (O) and Alexa647 (R) in *CalipHluor*$_{Ly}$ obtained from direct excitation yielded O/R values. An analogous 3D surface plot of O/R values as a function of [Ca^{2+}] and pH showed a sigmoidal increase as a function of Ca^{2+} with a ~9 fold change in O/R at pH 7.2 (Fig. 1d). At lysosomal pH in *C. elegans*, i.e., pH 5.5, *CalipHluor*$_{Ly}$ showed a K_d of 7.2 μM. As expected, the percentage signal change upon chelating Ca^{2+} also decreases as acidity increases (Fig. 1d).

In vivo performance of *CalipHluor*.

Next, we investigated the *in vivo* reporter characteristics of *CalipHluor*$_{Ly}$ as a function of lumenal pH and [Ca^{2+}]. When DNA-based reporters are injected into the pseudocoelom in *C. elegans* they are specifically uptaken by coelomocytes through the scavenger receptors mediated endocytosis and thereby label organelles on the endolysosomal pathway[21,24]. After labeling endocytic organelles with *CalipHluor*$_{Ly}$ thus, we clamped lumenal pH and [Ca^{2+}] of coelomocytes. This was achieved by incubating worms in clamping buffers of fixed pH and [Ca^{2+}] containing nigericin, monensin, ionomycin and EGTA at high [K^+] which clamped the endosomal ionic milieu to that of the surrounding buffer (Methods) [13,15,22,24]. Post-clamping, the worms were then imaged in four channels; (i) the donor channel (D or Alexa 488) (ii) the FRET acceptor channel (A), which corresponds to the intensity image of A647 fluorescence upon exciting A488, (iii) the orange channel (O or Rhod-5F), and (iv) the red channel (R) which corresponds to the intensity image of A647 fluorescence upon directly exciting Alexa 647. Fig. 2a (**i – iv**) shows representative images of a *CalipHluor*$_{Ly}$ labeled coelomocyte imaged in the four channels.

In a given clamping buffer of specified pH and Ca^{2+} concentration, the ratio of the donor channel (D) image to the acceptor channel (A) image yields a D/A image which corresponds to the clamping buffer pH (Fig. 2a (**v**)). Similarly, the O/R image corresponds to the Ca^{2+} concentration at that pH (Fig. 2a (**vi**)). Representative D/A and O/R images of coelomocytes clamped at the indicated pH and [Ca^{2+}] are shown in Figure 2b (Methods)(Supplementary Fig. S3). The distribution of D/A and O/R values of lysosomes clamped at different indicated pH and [Ca^{2+}] values are shown in Figures 2c–d. To compare the *in vivo* and *in vitro* sensing performances of both ion-sensing modules across a wide range of pH and Ca^{2+} we plotted two parameters for each module in *CalipHluor*$_{Ly}$. For the pH sensing module these were the fold change in D/A ($FC_{D/A}$), as well as the transition pH ($pH_{1/2}$) (Fig. 2e–f, Supplementary Fig. S4 a–d). For the Ca^{2+} sensing module, these were the fold change in O/R ($FC_{O/R}$) as well as the K_d for Ca^{2+} (Fig. 2g - h). The values of $FC_{D/A}$, $FC_{O/R}$, $pH_{1/2}$ and

K_d *in vivo* and *in vitro* were consistent revealing that the *in vitro* performance characteristics of *CalipHluor*$_{Ly}$ was quantitatively recapitulated *in vivo* (Fig. 2e–f and Fig 2i–k).

Measuring [Ca^{2+}] in organelles of the endo-lysosomal pathway

Endosomal maturation, critical to both organelle function and cargo trafficking, is accompanied by progressive acidification of the organelle lumen (Fig. 3a)[31,32]. Unlike pH, little is known about lumenal Ca^{2+} changes as a function of endosomal maturation[16,17]. We therefore sought to demonstrate the applicability of our probe across a range of acidic organelles by mapping lumenal Ca^{2+} as a function of endosomal maturation. We determined the time points at which *CalipHluor*$_{Ly}$ localized in the early endosome, the late endosome and the lysosome in coelomocytes as described previously [21] (Fig. 3b–c). Post injection, *CalipHluor*$_{Ly}$ was found to localize in early endosomes (EE), late endosomes (LE) and lysosomes (LY) at 5, 17 and 60 mins respectively (Fig. 3b–c, Supplementary Fig. S5).

We measured pH and apparent Ca^{2+} at each stage in wild type N2 nematodes with single endosome addressability using our probes. We then incorporated a K_d correction factor for each endosome according to its measured pH, and then computed the true value of Ca^{2+} in every endosome. Figure 3d shows a representative set of coelomocytes for which this method of analysis was performed. We labeled early and late endosomes with *CalipHluor* whereas we labeled lysosomes with the *CalipHluor*$_{Ly}$ variant and then generated the D/A and O/R maps of coelomocytes (Methods, Fig. 3d (**i**) & (**iv**)). The D/A map was directly converted into a pH map using the calibrated D/A values obtained from the *in vivo* pH clamping experiments (Fig. 3d(**ii**), Supplementary Table S2). The *in vivo* and *in vitro* Ca^{2+} response characteristics at every pH (Fig. 2h), provides the K_d for Ca^{2+} at every pH value for both *CalipHluor* and *CalipHluor*$_{Ly}$.

Using the pH map in Fig. 3d (**ii**) we constructed a "K_d map" which corresponds to the K_d for Ca^{2+} at each pixel in the pH map (Fig. 3d (**iii**), Supplementary Methods). Multiplying the value of K_d at each pixel in the K_d map with the equation $(O/R - O/R_{min})/(O/R_{max}-O/R)$ we obtain the true Ca^{2+} map (Fig. 3d(**v**)). In this equation, O/R corresponds to the observed O/R value at a given pixel in the O/R map, O/R_{min} and O/R_{max} correspond to O/R values at 1 μM and 10 mM Ca^{2+} at the corresponding pH value at that particular pixel. We thus obtained pH and Ca^{2+} maps of early endosomes, late endosomes and lysosomes in N2 worms (Fig. 3e) and the corresponding distributions of D/A and pH-corrected O/R are shown in Figures 3f–g. The mean values of pH and Ca^{2+} in each endosomal stage is shown in Figures 3h - i.

As expected, pH decreases progressively with endosomal maturation, with lumenal acidity showing a ~3-fold decrease at each endocytic stage. In contrast, Ca^{2+} in the early endosome and the late endosome were comparable and fairly low i.e., 0.3 μM. Interestingly, from the late endosome to the lysosome, lumenal Ca^{2+} increases sharply by ~35 fold, indicating a stage-specific enrichment of Ca^{2+} and consistent with the lysosome being an acidic Ca^{2+} store (Supplementary Table S3). The 100-fold difference between lysosomal and cytosolic Ca^{2+} is consistent with the stringent regulation of lysosomal Ca^{2+} channels to release lumenal Ca^{2+} and control lysosome function.

Catp-6 is identified as a potential lysosomal Ca^{2+} importer

This surge in lumenal Ca^{2+} specifically in the lysosome stage, implicates the existence of factors that aid lysosomal import of Ca^{2+}. However, players that mediate lysosomal Ca^{2+} accumulation are still unknown in higher eukaryotes. We took inspiration from the well-known Ca^{2+} importer i.e., SERCA, a P-Type ATPase which is present on the endoplasmic reticulum (ER)[25]. Other Ca^{2+} importers like plasma membrane Ca^{2+} ATPase (PMCA) and the secretory pathway Ca^{2+} ATPase (SPCA1) are also P-type-ATPases[33]. Therefore we manually identified potential P-type ATPases in the human lysosomal proteome [34–38]. We found the P5-ATPase ATP13A2 was described to transport cations like Mn^{2+}, Zn^{2+}, Mg^{2+}, and Cd^{2+} but not Ca^{2+} based on toxicity assays[26]. As Ca^{2+} homeostasis is critical to all major signaling pathways, compensatory mechanisms in cells can counter excess Ca^{2+} and thereby omit the identification of Ca^{2+} transport by ATP13A2.

C. elegans has two homologs of ATP13A2 i.e., *catp-5* and *catp-6* (Fig. 4a). To test whether *catp-6* mediated lysosomal Ca^{2+} accumulation, we investigated whether its knockdown would rescue a phenotype arising due to high lumenal Ca^{2+} (Fig. 4b). TRPML1 is a well-known lysosomal Ca^{2+} release channel whose knockdown would be expected to elevate lysosomal Ca^{2+}[39,40]. Mutations in TRPML1 result in lysosomal dysfunction that leads to the lysosomal storage disease Mucopolysaccharidoses Type IV (MPS IV) [41]. In *C. elegans*, loss of *cup-5*, the *C. elegans* homolog of TRPML1, results in lysosomal storage and embryonic lethality [42]. We therefore tested whether *catp-6* knockdown a *cup-5+/−* genetic background could reverse *cup-5 −/−* lethality. In this strain, the homozygous lethal deletion of *cup-5* is balanced by *dpy-10* marked translocation [43]. We performed a survival assay by knocking down specific genes in *cup-5+/−* worms and scoring for lethality (Fig. 4c and Supplementary Fig S6).

Multidrug resistance protein-4 (MRP-4) is a versatile efflux transporter for drugs, toxins, peptides and lipids and is known to rescue *cup-5−/−* lethality [44]. It is hypothesized that in the absence of *cup-5, mrp-4* mis-localizes in endocytic compartments causing toxicity that is then alleviated upon its knockdown. RNAi knockdown of either *catp-6* or *catp-5* rescued *cup-5−/−* lethality favorably compared to *mrp-4* knockdown (Supplementary Fig S6). Knocking down *clh-6*, another lysosome-resident channel that regulates lumenal chloride, showed no such rescue[24,28].

Catp-6 facilitates lysosomal Ca^{2+} accumulation—Given that the rescue of lethality might occur without restoring lysosomal function, we tested whether any of our candidate genes reversed lysosomal phenotypes. *Cup-5* knockdowns show abnormally large lysosomes due to lysosomal storage [28]. We therefore used the hypomorph *ar645* with a G401E mutation in *cup-5* leading to dysfunction that is insufficient for lethality, yet leads to engorged lysosomes[45]. In the *arIs37*;*cup-5(ar465)* strain, soluble GFP that is secreted from the muscle cells into the pseudocoelom is internalized by the coelomocytes and trafficked for degradation to dysfunctional lysosomes[45]. Thus, in these worms, the lysosomes in coelomocytes are abnormally enlarged and labeled with GFP (Fig. 4d).

RNAi knockdowns of *catp-6* in these nematodes rescued lysosomal morphology (Fig. 4d–e, Methods). Knocking down either *catp-5* or *mrp-4* showed only a marginal recovery of

phenotype. Given that *mrp-4* is not a lysosome resident protein and its inability rescue the lysosomal phenotype suggests that mechanistically, its rescue of *cup-5 −/−* lethality is likely to be extra lysosomal, consistent with previous hypotheses.

We then checked whether *catp-6*-mediated rescue of a physical phenotype i.e., lysosome morphology, also led to a restoration of a chemical phenotype, i.e., its lumenal Ca^{2+}. Lysosomal Ca^{2+} measurements using $CalipHluor_{Ly}$ in *cup-5* +/− nematodes and in *catp-6* knockdowns we made. Wild type nematodes showed lysosomal Ca^{2+} levels of 11 ± 0.8 μM (Fig. 4f–h). In *cup-5 +/−* nematodes lysosomal Ca^{2+} was elevated to 40 ± 1.5 μM, consistent with *cup-5* being a Ca^{2+} release channel (Fig. 4f–h). Interestingly, *catp-6* knockdown restored lysosomal Ca^{2+} to wild-type levels. Thus *catp-6* function directly opposes that of *cup-5* as it rescues *cup-5* deficient phenotypes at three levels - the whole organism in terms of lethality, at the sub-cellular level in terms of lysosome phenotype, at sub-organelle level in terms of its lumenal chemical composition. Cumulatively, these indicate that *catp-6* facilitates lysosomal Ca^{2+} import. Accordingly, *catp-6* deletion led to lysosomal Ca^{2+} dropping to 1.6 ± 0.4 μM, consistent with it facilitating Ca^{2+} import.

ATP13A2 facilitates lysosomal Ca^{2+} accumulation.

Mutations in ATP13A2, the human homolog of *catp-6*, belong to the PARK9 Parkinsons disease susceptibility locus. These mutations lead to the Kufor- Rakeb syndrome, a severe, early onset, autosomal recessive form of Parkinsons disease with dementia [46]. Parkinsons disease is strongly connected to Ca^{2+} dysregulation since excessive cytosolic Ca^{2+} causes excitotoxicity of dopaminergic neurons [47]. Interestingly, overexpressing ATP13A2 suppresses toxicity and reduces cytosolic Ca^{2+} [27,48]. Further, loss of ATP13A2 function leads to neuronal ceroid lipofuscinosis, a lysosomal storage disorder, implicating the lysosome as its potential site of action [49].

To confirm whether i.e., ATP13A2, also facilitated lysosomal Ca^{2+} import, we mapped lysosomal Ca^{2+} in human fibroblasts. We created a variant called $CalipHluor^{mLy}$ suited to measure the high acidity of mammalian lysosomes (Supplementary Fig. S7a). $CalipHluor^{mLy}$ showed similar pH and Ca^{2+} response characteristics *in vitro*, on beads and *in cellulo* and its Ca^{2+} sensing characteristics are unaffected by the new pH sensing module (Supplementary Fig. S7b - e)

We then localized $CalipHluor^{mLy}$ in lysosomes of primary human dermal fibroblasts (HDF cells) obtained from punch-skin biopsies. We showed that $CalipHluor^{mLy}$ labels lysosomes in HDF cells by scavenger receptor mediated endocytosis (Fig. 5a–b Supplementary Fig. S8). Briefly, a 1 h pulse of 500 nM $CalipHluor^{mLy}$ followed by a 9 h chase efficiently labels lysosomes in this cell type (Fig. 5a–b).

We then measured lysosomal Ca^{2+} in fibroblasts from normal individuals and L6025 primary fibroblasts isolated from male patients with Kufor Rakeb syndrome, that are homozygous for a C>T mutation in 1550 of ATP13A2 [50]. This mutation results in ATP13A2 being unable to exit the ER and the lysosomes are devoid of ATP13A2[50]. After confirming its lysosomal localization in L6025 cells, using $CalipHluor^{mLy}$ we measured lysosomal pH and Ca^{2+} (Fig. 5b–d). Lysosomes in KRS patients showed 14-fold lower Ca^{2+} and ~2-fold

lower [H^+] than normal (Fig. 5c–e) confirming that ATP13A2 mediates lysosomal Ca^{2+} accumulation.

Conclusion

Small molecule as well as genetically encodable Ca^{2+} indicators have profoundly impacted biology. However, their pH sensitivity has restricted their use to the cytoplasm or the endoplasmic reticulum, where the pH is neutral and fairly constant. Ca^{2+} mapping of acidic microenvironments has therefore not been previously possible. Our DNA-based fluorescent reporter, *CalipHluor*, combines the photophysical advantages of small molecule Ca^{2+} indicators with the precise organelle targetability of endocytic tracers. *CalipHluor* is a pH-correctable Ca^{2+} reporter that simultaneously reports pH and Ca^{2+} in organelles retaining concentration information on both ions with single organelle addressability. Thus, by knowing exactly how the affinity (the K_d) of the Ca^{2+} sensitive probe changes with pH, we compute the K_d at every pixel in the pH map to generate a K_d map. From the K_d map and the O/R map, we can construct the true Ca^{2+} map of the acidic organelle.

Given the newfound ability to directly quantitate lysosomal Ca^{2+} using *CalipHluor*, we identified ATP13A2 - a risk gene for Parkinson's disease - as a potential lysosomal Ca^{2+} importer. We found that the function of *catp-6*, the *C. elegans* homolog of ATP13A2, directly opposed that of a well-known lysosome-resident Ca^{2+} release channel, *cup-5*. It reversed *cup-5* phenotypes at three different levels – a whole organism phenotype, a sub-cellular phenotype and an intra-lysosomal phenotype. This now provides a framework to identify more lysosomal Ca^{2+} regulators.

The ability to map pH and Ca^{2+} with single organelle addressability is critical to discriminate between lysosomal hypo-acidification and Ca^{2+} dysregulation. *CalipHluor* can be used to map lumenal Ca^{2+} changes in diverse organelles. There is already a range of DNA-based pH sensors specifically suited to organelles like the Golgi, the recycling endosome and the ER [19,20,22–24]. Given the array of small molecule Ca^{2+} indicators covering various Ca^{2+} affinities, this positions *CalipHluor* technology to deliver new insights into organellar Ca^{2+} regulation.

Online Methods

Preparation of BAPTA-5F aldehyde (1)

BAPTA-5F aldehyde (**1**) was synthesized according to previous reported procedure [51,52]. $POCl_3$ (1.12g, 7.3 mmol) was added to DMF (5 mL) at 0 °C and allowed to stir for 10 min. After 10 min, BAPTA-5F (1.6 g, 2.9 mmol) in DMF (3mL) was added to above solution and heated to 65 °C. After completion of the reaction, reaction mixture was poured in water and pH adjusted to 6.0 by adding aq. NaOH (1M) solution. Product was extracted with ethylacetate (3×50 mL) and solvent was evaporated. Crude product was purified by column chromatography on silica gel using hexane/EtOAc (70/30 to 60/40) as an eluent to obtain BAPTA-5F aldehyde (**1**) in 65% yield. ^{1}H-NMR (500 MHz, $CDCl_3$) δ_{ppm} 9.80 (s, 1H), 7.30–7.45 (m, 2H), 6.83 (t, 1H, J = 7 Hz), 6.76 (d, 1H, J = 8 Hz), 6.59 (t, 2H, J = 8 Hz), 4.40 (t, 2H, J = 7.0 Hz), 4.35 (t, 2H, J = 7.5 Hz), 4.33 (s, 4H), 4.22 (s, 4H), 3.59 (s, 6H), 3.57 (s,

6H). ^{13}C-NMR (125 MHz, $CDCl_3$) δ_{ppm} 190.5, 171.8, 171.2, 159.4, 157.5, 151.4, 151.3, 149.6, 145.1, 135.6, 135.5, 130.0, 126.9, 120.3, 120.2, 116.6, 110.8, 107.3, 107.1, 101.3, 101.1, 67.1, 67.0, 53.5, 53.4, 51.9, 51.7. HRMS (ESI) *m/z*: $[M]^+$ calcd for $C_{27}H_{31}FN_2O_{11}^+$ 578.1912, found: 578.1927.

Synthesis of Rhod-5F

To a solution of BAPTA-5F aldehyde (**1**) (50 mg, 0.086 mmol) in propionic acid (4 mL), 3-(dimethylamino) phenol (26 mg, 0.19 mmol) and p-Toluenesulfonic acid (p-TSA) (1.5 mg, 0.009 mmol) were added and allowed to stir at room temperature for 12 h. After 12 h, Chloranil (21 mg, 0.086 mmol) in DCM (3 mL) was added to above reaction mixture and allowed to stir at room temperature overnight. After completion of the reaction, the crude product was extracted with DCM (3×30 mL). The crude product was then purified by column chromatography on silica gel using DCM/Methanol (95/5 to 90/10 %) as an eluent to obtain methyl ester of Rhod-5F as a dark red solid in 35 % yield. LCMS (ESI) *m/z*: $[M]^+$ calcd for $C_{43}H_{48}FN_4O_{11}^+$ 815.3298, found: 815.5. Methyl ester of Rhod-5F (5 mg, 0.006 mmol) was dissolved in methanol and water mixture (1:0.5 mL), to which KOH (3.5 mg, 0.063mmol) was added and allowed to stir for 8 h at room temperature. After completion of the reaction, solution pH was adjusted to 6.0 and crude product was extracted with DCM (3×5 mL). Product was purified by HPLC (50:50 acetonitrile/water, 0.1 % TFA) to obtained Rhod-5F. LCMS (ESI) *m/z*: $[M]^+$ calcd for $C_{39}H_{40}FN_4O_{11}^+$ 759.2672, found: 759.4.

Preparation of 1-azido-3-iodopropane (2)

To a solution of 1-bromo-3-chloropropane (1 g, 6.4 mmol) in DMSO (8 mL), sodium azide (0.5 g, 7.7 mmol) was added and allowed to stir at room temperature for 12 h. After completion of the reaction, the mixture was diluted with water and the product was extracted with hexane to obtain 1-azido-3-chloropropane. Sodium iodide (1.5 g, 10 mmol) was then added to a solution of 1-azido3-chloropropane (1 g, 8.4 mmol) in acetone (25 mL) and allowed to stir at room temperature for 8 h. After completion of the reaction, the solvent was evaporated under vacuum. The crude product was diluted with a saturated solution of $Na_2S_2O_3$ to quench the unreacted iodine followed by extraction of the compound with ethyl acetate (3×50 mL). This was dried over Na_2SO_4 and the product 1-azido-3-iodopropane (**2**) was used for further reactions without purification.

Preparation of 3-((3-azidopropyl)(methyl)amino)phenol (3)

To a solution of 3-aminophenol (1 g, 9.2 mmol) in acetone (30 mL), potassium carbonate (2.5 g, 18.4 mmol) was added and allowed to stir at room temperature for 20 min. After 20 min, iodomethane (1.3 g, 9.2 mmol) was added and the mixture was further stirred for 8 h at room temperature. After completion of reaction, the solvent was evaporated and the crude product was extracted with DCM (3×30 mL). This was followed by purification of the crude product by column chromatography on silica gel using hexane/ethyl acetate (80/20 %) as an eluent to obtained 3-(methylamino) phenol in 45 % yield.

To a solution of 3-(methylamino) phenol (1 g, 8.1 mmol) in DMF (8 mL), N, N-Diisopropylethylamine (1.26 g, 9.7 mmol) was added and stirred for 20 min at room temperature. After 20 min, 1-azido-3-iodopropane (**2**) (1.7 g, 8.1 mmol) was added to above

reaction mixture and heated at 65 °C for 8 h. After completion of the reaction, the solvent was evaporated and the crude product was extracted with diethylether (3×40 mL). Then, the crude product was purified by column chromatography on silica gel using hexane/ethyl acetate (90/10 %) as an eluent to obtained 3-((3-azidopropyl)(methyl)amino)phenol (**3**) liquid in 72 % yield. ^{1}H-NMR (500 MHz, $CDCl_3$) δ_{ppm} 7.09–7.13 (m, 1H), 6.3 (d, 1H, J = 7.5 Hz), 6.21 (dd, 2H, J = 2 Hz, 8.5 Hz), 3.42 (t, 2H, J = 6.5 Hz), 3.38 (t, 2H, J = 7 Hz), 2.94 (s, 3H), 1.87 (t, 2H, J = 6.5 Hz). ^{13}C-NMR (125 MHz, $CDCl_3$) δ_{ppm} 156.7, 150.7, 130.2, 105.1, 103.5, 99.3, 49.8, 49.2, 38.6, 26.3. HRMS (ESI) *m/z*: $[M]^+$ calcd for $C_{10}H_{14}N_4O^+$ 206.1168, found:206.1177

Preparation of Rhod-5F-OMe (4)

To a solution of BAPTA-5F aldehyde (**1**) (50 mg, 0.086 mmol) in propionic acid (4 mL), 3-((3-azidopropyl)(methyl)amino)phenol (**3**) (40 mg, 0.19 mmol) and p-Toluenesulfonic acid (p-TSA) (1.5 mg, 0.009 mmol) were added and allowed to stir at room temperature for 12 h. After 12 h, Chloranil (21 mg, 0.086 mmol) in DCM (3 mL) was added to above reaction mixture and allowed to stir at room temperature overnight. After completion of the reaction, the solvent was evaporated and the crude product was extracted with DCM (3×20 mL). The crude product was then purified by column chromatography on silica gel using DCM/Methanol (95/5 to 90/10 %) as an eluent to obtain Rhod-5F-OMe (**4**) as a dark red solid in 30 % yield. ^{1}H-NMR (500 MHz, DMSO-d_6) δ_{ppm} 7.55 (d, 2H, J = 8 Hz), 7.15–7.16 (m, 3H), 7.00–7.04 (m, 3H), 6.88 (dd, 2H, J = 3 Hz, 9 Hz), 6.75 (dd, 1H, J = 6 Hz, 9 Hz), 6.65 (td, 1H, J = 3 Hz, 6 Hz), 4.20–4.30 (m, 8H), 4.02 (s, 4H), 3.71 (t, 4H, J = 7 Hz), 3.53 (s, 6H), 3.47 (s, 10H), 3.25 (s, 6H), 1.88 (q, 4H, J = 7 Hz). ^{13}C-NMR (125 MHz, DMSO-d_6) δ_{ppm} 171.2, 171.1, 158.3, 157.3, 156.4, 156.1, 140.7, 135.2, 135.1, 131.9, 123.6, 123.1, 119.1, 116.8, 114.9, 114.4, 106.4, 106.2, 101.2, 101.0, 96.4, 67.3, 67.2, 54.9, 53.2, 53.0, 51.5, 51.2, 49.7, 48.6, 48.1, 26.0, 22.1. HRMS (ESI) *m/z*: $[M]^+$ calcd for $C_{47}H_{54}FN_{10}O_{11}^+$ 953.3952, found: 953.3967.

Preparation of Rhod-5F-N_3

Rhod-5F-OMe (**4**) (5 mg, 0.005 mmol) was dissolved in methanol and water mixture (1:0.5 mL), to which KOH (3.5 mg, 0.063mmol) was added and allowed to stir for 8 h at room temperature. After completion of the reaction, solution pH was adjusted to 6.0 and crude product was extracted with DCM (3×5 mL). Product was purified by HPLC (50:50 acetonitrile/water, 0.1 % TFA). LCMS (ESI) *m/z*: $[M]^+$ calcd for $C_{43}H_{46}FN_{10}O_{11}^+$ 897.3326, found: 897.5.

Reagents

All the chemicals used for the synthesis of Rhod-5F-N_3 were purchased from Sigma (USA) and Alfa Aesar (USA). ^{1}H-NMR and ^{13}C-NMR were recorded on Bruker AVANCE II+, 500MHz NMR spectrophotometer in $CDCl_3$ and DMSO-d_6 and tetramethylsilane (TMS) used as an internal stranded. Mass spectra were recorded in Agilent 6224 Accurate-Mass TOF LC/MS.

All fluorescently labeled oligonucleotides were purchased from IDT (USA) and IBA-GmBh (Germany). HPLC purified oligonucleotides were dissolved in Milli-Q water to make 100

μM stock solutions and quantified using UV-spectrophotometer and stored at −20 °C. Ethylene glycol-bis(β-aminoethyl ether)-N,N,N,N -tetraacetic acid (EGTA), ampicillin, carbencillin, isopropyl β-D-1-thiogalactopyranoside (IPTG), nigericin and monensin were purchased from Sigma (USA) and ionomycin was obtained from Cayman chemical (USA). Maleylated BSA (mBSA) was maleylated according to a previously published protocol[20]. Monodisperse Silica Microspheres were obtained from Cospheric (USA).

Rhod-5F conjugation and sample preparation

Rhod-5F was first conjugated to D2 and O3-DBCO strands. Rhod-5F-N_3 (25 μM) was added to 5 μM of dibenzocyclooctyne (DBCO) labelled D2 strand in 100 μL of sodium phosphate (10 mM) buffer containing KCl (100 mM) at pH 7.0 and allowed to stir overnight at room temperature. After completion of the reaction, 10 μL of 3 M sodium acetate (pH 5.5) and 250 μL of ethanol were added to reaction mixture and kept overnight at −20 °C for DNA precipitation [53]. Then, the reaction mixture was centrifuged at 14000 rpm at 4 °C for 20 min to remove the unreacted Rhod-5F-N_3 and the precipitate was resuspended in ethanol and centrifuged. This procedure was repeated 3 times for complete removal of unreacted Rhod-5F-N_3. Rhod-5F conjugation was confirmed by gel electrophoresis by running a native polyacrylamide gel containing 15% (19:1 acrylamide/bis-acrylaimde) in 1X TBE buffer [Tris.HCl (100 mM), boric acid (89 mM) and EDTA (2 mM), pH 8.3]. The same protocol was used for the conjugation of Rhod-5F-N_3 to O3-DBCO.

To prepare a *CalipHluor*$_{Ly}$ and *CalipHluor*^{mLy} sample, 5 μM of D1 or OG-D1 and 5 μM of Rhod-5F conjugated D2 strands were mixed in equimolar ratios in 10 mM sodium phosphate buffer (pH 7.2) containing 100 mM of KCl. The resultant solution was heated to 90 °C for 15 min, cooled to room temperature at 5 °C per 15 min and kept at 4 °C for overnight [20]. For *CalipHluor*, 5 μM of O1-A488, 5 μM of O2-A647 and 5 μM of Rhod-5F conjugated O3 strands were mixed in equimolar ratios in 10mM sodium phosphate buffer at pH 5.5 containing 100 mM of KCl. Solution was heated to 90 °C for 15 min, then cooled to room temperature at 3 °C per 15 min and kept at 4 C for overnight. See table S1 for sequence information.

In vitro fluorescence measurements

Fluorescence spectra were measured on a FluoroMax-4 spectrophotometer (Horiba Scientific, Edison, NJ, USA) using previously established protocols [20]. For *in vitro* pH measurements, *CalipHluor*$_{Ly}$ sample was diluted to 30 nM in pH clamping buffer [$CaCl_2$ (50 μM to 10 mM), HEPES (10 mM), MES (10 mM), sodium acetate (10 mM), EGTA (10 mM), KCl (140 mM), NaCl (5 mM) and $MgCl_2$ (1 mM)] of desired pH and equilibrated for 30 min at room temperature. All the samples were excited at 495 nm and emission spectra was collected from 505 nm to 750 nm. The ratio of donor (D) emission intensity at 520 nm to acceptor (A) emission intensity at 665 nm was plotted as a function of pH to generate the pH calibration curve. Mean of D/A from two independent experiments and their s.e.m were plotted for each pH. Fold change in D/A of *CalipHluor*$_{Ly}$ was calculated from the ratios of D/A at pH 4.0 and pH 6.5. $pH_{1/2}$ of *CalipHluor*$_{Ly}$ at different [Ca^{2+}] values were derived from pH calibration curve by fitting to Boltzmann sigmoid.

For *in vitro* [Ca^{2+}] measurements, *CalipHluor*$_{Ly}$ sample was diluted to 30 nM in Ca^{2+} clamping buffer [HEPES (10 mM), MES (10 mM), sodium acetate (10 mM), EGTA (10 mM), KCl (140 mM), NaCl (5 mM) and $MgCl_2$ (1 mM)]. We then varied the amount of [Ca^{2+}] from 0 mM to 20 mM and adjusted to different pH values (4.5–7.20). The amount of free [Ca^{2+}] at a given pH was calculated based on Maxchelator software (http://maxchelator.stanford.edu/). Rhod-5F and Alexa 647 were excited at 545 nm and 630 nm respectively. Emission spectra for Rhod-5F (O) and Alexa 647 (R) were collected from 570–620 nm and 660–750 nm respectively. Mean of O/R from two independent experiments and their s.e.m were plotted for each [Ca^{2+}]. Similar experiments were performed with 50nM *CalipHluor*^{mLy} at pH 4.6 and pH 5.1. *In vitro* calcium binding affinity (K_d) of Rhod-5F was obtained by plotting ratios of Rhod-5F (O) emission intensity at 580 nm to Alexa 647 (R) emission intensity at 665 nm as a function of free [Ca^{2+}] and fitted using sigmoidal growth Hill1 equation.

$$Y = S + (E - S) \times (X^n/(K_d^n + X^n)) \quad (1)$$

X is free [Ca^{2+}], Y is O/R ratio at given free [Ca^{2+}], S is O/R ratio at low [Ca^{2+}], E is O/R ratio at high [Ca^{2+}], K_d is dissociation constant and n is Hill coefficient. Fold change response in O/R of *CalipHluor*$_{Ly}$ was calculated from ratio of O/R at high [Ca^{2+}] and O/R at low [Ca^{2+}].

C.elegans methods and strains

Standard methods were followed for the maintenance of *C. elegans* [54]. Wild type strain used was the *C. elegans* isolate from Bristol, strain N2 (Brenner, 1974). Strains used in the study, provided by the Caenorhabditis Genetics Center (CGC), are RRID:WB-STRAIN:RB2510 W08D2.5(ok3473) and RRID:WBSTRAIN:VC1242 *[+/mT1 II; cup-5(ok1698)/mT1 [dpy-10(e128)] III*]. Transgenics used in this study, also provided by the CGC, are RRID:WB-STRAIN:NP1129 *cdIs131 [pcc1::GFP::rab-5 + unc-119(+) + myo-2p::GFP]*, a transgenic strain that express GFP-fused early endosomal marker RAB-5 inside coelomocytes, RRID:WB-STRAIN:NP871 *cdIs66 [pcc1::GFP::rab-7 + unc-119(+) + myo-2p::GFP]*, a transgenic strain that express GFP-fused late endosomal / lysosomal marker RAB-7 inside coelomocytes RRID:WB-STRAIN:RT258 *pwIs50 [lmp-1::GFP + Cbr-unc-119(+)]*, a transgenic strain expressing GFP-tagged lysosomal marker LMP-1 and *arIs37[myo-3p::ssGFP + dpy-20(+)]I*, a transgenic strain that express ssGFP in the body muscles which secreted in pseudocoelom and endocytosed by coelomocytes and *arIs37[myo-3p::ssGFP + dpy-20(+)]Icup5(ar465)* a transgenic strain with enlarged GFP containing vesicles in coelomocytes due to defective degradation. Gene knocked down was performed using Ahringer library-based RNAi methods [55]. The RNAi clones used were: L4440 empty vector control, *catp-6* (W08D2.5, Ahringer Library), *catp-5* (K07E3.7, Ahringer Library) and *mrp-4* (F21G4.2, Ahringer Library).

CalipHluor trafficking in coelomocytes

CalipHluor trafficking in coelomocytes was done in transgenic strains expressing endosomal markers such as GFP::RAB-5 (EE), GFP::RAB-7 (LE) and LMP-1::GFP (Ly) as described

previously by our lab [21]. Briefly, worms were injected with *CalipHluor*$_{A647}$ (500 nM) and incubated for specific time points and transferred on to ice. Worms were anaesthetized using 40 mM of sodium azide in M9 solution. Worms were then imaged on Leica TCS SP5 II STED laser scanning confocal microscope (Leica Microsystems, Inc., Buffalo Grove, IL) using an Argon ion laser for 488 nm excitation and He-Ne laser for 633nm excitations with a set of filters suitable for GFP and Alexa 647 respectively. Colocalization of GFP and *CalipHluor*$_{A647}$ was determined by counting the number *CalipHluor*$_{A647}$ positive puncta that colocalize with GFP-positive puncta and quantified as a percentage of total number of *CalipHluor*$_{A647}$ positive puncta[21]. In order to confirm lysosomal labeling in a given genetic background, the same procedure was performed on the relevant mutant or RNAi knockdown in *pwIs50 [lmp-1::GFP + Cb-unc-119(+)].*

RNAi experiments

Bacteria from the Ahringer RNAi library expressing dsRNA against the relevant gene was fed to worms, and measurements were carried out in one-day old adults of the F1 progeny (Kamath and Ahringer, 2003). RNA knockdown was confirmed by probing mRNA levels of the candidate gene, assayed by RT-PCR. Briefly, total RNA was isolated using the Trizol-chloroform method; 2.5 μg of total RNA was converted to cDNA using oligo-dT primers. 5 μL of the RT reaction was used to set up a PCR using gene-specific primers. Actin mRNA was used as a control. PCR products were separated on a 1.5% agarose-TAE gel.

Image acquisition

Image acquisition was carried out on wide field IX83 inverted microscope (Olympus Corporation of the Americas, Center Valley, PA, USA) using a 60X, 1.42 NA, phase contrast oil immersion objective (PLAPON, Olympus Corporation of the Americas, Center Valley, PA, USA) and Evolve Delta 512 EMCCD camera (Photometrics, USA). Filter wheel, shutter and CCD camera were controlled using Metamorph Premier Ver 7.8.12.0 (Molecular Devices, LLC, USA), suitable for the fluorophores used. Images on the same day were acquired under the same acquisition settings. Alexa 488 channel images (D) were obtained using 480/20 band pass excitation filter, 520/40 band pass emission filter and 89016-ET-FITC/Cy3/Cy5 dichroic filter. Alexa 647 channel images (A) were obtained using 640/30 band pass excitation filter, 705/72 band pass emission filter and 89016ET-FITC/Cy3/Cy5 dichroic filter. FRET channel images were obtained using the 480/20 band pass excitation filter, 705/72 band pass emission filter and 89016-ET-FITC/Cy3/Cy5 dichroic filter. Rhod-5F channel images (O) were obtained using 545/25 band pass excitation filter, 595/50 band pass emission filter and a 89016-ET-FITC/Cy3/Cy5 dichroic filter. Confocal images were acquired on a Leica TCS SP5 II STED laser scanning confocal microscope (Leica Microsystems, Inc., Buffalo Grove, IL, USA) equipped with 63X, 1.4 NA, oil immersion objective. Alexa 488 was excited using an Argon ion laser for 488 nm excitation, Alexa 647 using He-Ne laser for 633 excitation and Rhod-5F using DPSS laser for 561 nm excitation with a set of dichroics, excitation, and emission filters suitable for each fluorophore.

Image analysis

Image analysis for quantification of pH and calcium in single endosomes was done using custom MATLAB code. For each cell the most focused plane was manually selected in the

Alexa 647 channel. This image and corresponding images from the same z-position in other channels were input into the program. Images from the different channels were then aligned using Enhanced Cross Correlation Optimization [56]. To determine the location of the endosome first a low threshold was used to select the entire cell. Only the area within the cell was subsequently considered for endosome selection. Regions of interest corresponding to individual endosomes were selected in the Alexa 647 channel by adaptive thresholding using Sauvolas method [57]. The initial selection was further refined by watershed segmentation and size filtering. After segmentation regions of interest were inspected in each image and selection errors were corrected manually. Using the cell boundary annular region 10 pixels wide around the cell was selected and used to calculate a background intensity in each image. Then, we measured the mean fluorescence intensity in each endosome in donor (D), acceptor (A), Rhod-5F (O) and Alexa 647 (R) channels and the background intensity corresponding to that cell and channel was subtracted. The two ratios of intensities (D/A and O/R) were then computed for each endosome. Mean D/A of each distribution was plotted as a function of pH and obtained the *in vivo* pH calibration curve. Mean O/R of each distribution was plotted as a function of free [Ca^{2+}] to generate the *in vivo* Ca^{2+} calibration curve. Pseudo color pH and Ca^{2+} images were obtained by measuring the D/A and O/R ratio per pixel, respectively.

In vivo measurements of pH and [Ca^{2+}]

In vivo pH calibration experiments of *CalipHluor*$_{Ly}$ were carried out using protocols previously established in our lab (Modi *et al.*, 2009; Surana *et al.*, 2011). Briefly, *CalipHluor*$_{Ly}$ (500 nM) was microinjected in pseudocoelom of young adult worms on the opposite side of the vulva. After microinjections, worms were incubated at 22 °C for 2 h for maximum labelling of coelomocyte lysosomes. Then, worms were immersed in clamping buffer [$CaCl_2$ (50 μM to 10 mM), HEPES (10 mM), MES (10 mM), sodium acetate (10 mM), EGTA (10 mM), KCl (140 mM), NaCl (5 mM) and $MgCl_2$ (1 mM)] of desired pH solutions containing the ionophores nigericin (50 μM), monensin (50 μM) and ionomycin (20 μM). Worm cuticle was perforated to facilitate the entry of buffer in to the body. After 75 min of incubations in clamping buffer, coelomocytes were imaged using wide-field microscopy. Three independent measurements, each with 10 worms, were made for each pH value.

Ca^{2+} clamping measurements were carried out using *CalipHluor*$_{Ly}$. Worms were injected with *CalipHluor*$_{Ly}$ (500 nM) and incubated at 22 °C for 2 h. After 2 h, worms were immersed in Ca^{2+} clamping buffer [HEPES (10 mM), MES (10 mM), sodium acetate (10 mM), EGTA (10 mM), KCl (140 mM), NaCl (5 mM) and $MgCl_2$ (1 mM)] by varying amount of free [Ca^{2+}] from 1 μM to 10 mM and adjusted to different pH values (5.3–6.5). Three independent measurements, each with 10 worms, were made for Ca^{2+} value.

Early endosome and late endosome pH and free [Ca^{2+}] measurements were carried out using *CalipHluor*, and lysosomal pH and free [Ca^{2+}] measurements were carried out using *CalipHluor*$_{Ly}$. For real time pH and [Ca^{2+}] measurements, 10 hermaphrodites were injected with 500 nM of *CalipHluor* and *CalipHluor*$_{Ly}$ for EE, LE and Ly respectively and incubated for the indicated time points (EE (5 min), LE (17 min) and Ly (60 min)). Worms were

anaesthetized using 40 mM of sodium azide in M9 solution and imaged on wide field microscopy. Image analysis was carried out using custom MATLAB code as described in image analysis.

Calculating pH corrected [Ca^{2+}] in EE, LE and Ly

The D/A and O/R ratios in Ly, LE and EE were measured using *CalipHluor*$_{Ly}$ and *CalipHluor* as mentioned above at single endosome resolution. Over 100 endosomes were analyzed in each measurement in worms to generate a Gaussian spread of D/A. Around ~5%, endosomes which fell outside the range of Mean ± 2 S.D (S.D = standard deviation) which was set as a threshold for our measurements in EE, LE and Ly. To get pH corrected [Ca^{2+}] values, we measured the pH value in each individual endosome with single endosome resolution from their D/A ratios. pH values in endosomes were calculated using equation (2) which was derived from our *in vivo* pH calibration curve,

$$\mathrm{pH} = pH_{1/2} + [0.3\ln\left(\left(\frac{K_1 - K_2}{Y - K_2}\right) - 1\right)] \quad (2)$$

K_1, K_2 and $pH_{1/2}$ represent parameters derived from a Boltzmann fit of the *in vivo* pH calibration curve, and Y represents the D/A ratio in a given endosome.

Next, the K_d of *CalipHluor*$_{Ly}$ and fold change response in O/R ratios of *CalipHluor*$_{Ly}$ from low [Ca^{2+}] O/R to high [Ca^{2+}] were obtained as functions of pH. The *in vitro* and *in vivo* K_d were measured at different pH points ranging from 4.5 to 7.2 by fitting Ca^{2+} calibration curves by fitting to the Hill equation (1). From *in vitro* and *in vivo* [Ca^{2+}] calibration curves, the K_d of *CalipHluor*$_{Ly}$ was plotted as a function of pH using following equation,

$$\mathrm{K_d} = 1.03 + 5.14 \times 10^{12} \times e^{(-\frac{pH}{0.189})} + 3.108 \times 10^{6} \times e^{(-\frac{pH}{0.412})} \quad (3)$$

By using equation, we can deduce K_d of *CalipHluor*$_{Ly}$ at any given pH in EE, LE and Ly. O/R_{max} (i.e., O/R ratio at high [Ca^{2+}]), was obtained by clamping the worms at 10 mM of free [Ca^{2+}] at different pH points. *In vitro* and *in vivo* [Ca^{2+}] calibration curves showed that *CalipHluor*$_{Ly}$ retained its fold-change response of O/R from 1 μM to 10 mM at different pH points. O/R_{min} (i.e., O/R ratio at low [Ca^{2+}]) values were calculated from fold change response as function of pH and normalized to O/R_{max}.

$$\mathrm{O/R_{min}} = \frac{1}{4.24 + 0.12 \times \exp(0.5 \times pH)} \quad (4)$$

As mentioned above, the pH in EE, LE and Ly was measured from D/A by using equation (2) at single endosome resolution. pH and O/R, were used to calculate K_d and O/R_{min} from equation (3) and (4). Finally, K_d, O/R_{min}, O/R and O/R_{max} were substituted in the following equation to get pH corrected free [Ca^{2+}] values in endosome by endosome level.

$$\text{Free } [Ca^{2+}] = K_d \times \left[\frac{O/R - O/R_{min}}{O/R_{max} - O/R}\right] \quad (5)$$

Three independent measurements, each with 10 worms, were made for pH and $[Ca^{2+}]$ values in EE, LE and Ly.

Image analysis – pH corrected $[Ca^{2+}]$ images

High resolution images were acquired using confocal microscopy as mentioned in methods section. Images were acquired in four channels (Alexa 488, FRET, Rhod-5F and Alexa 647 channels) to quantify pH and $[Ca^{2+}]$ at single endosome resolution. To compensate for the pH component in Ca^{2+} measurements, the K_d of *CalipHluor*$_{Ly}$ at single endo-lysosomal compartments was calculated based on the K_d calibration plot discussed above. The pH of endo-lysosomes was quantified by measuring the donor/acceptor values calibrated across physiological pH (4.0–6.5). Donor (D) and acceptor (A) images were background subtracted by drawing an ROI outside the worms. Donor (D) image was duplicated and a threshold was set to create a binary mask. Background subtracted donor and acceptor images were then multiplied with the binary mask to get processed donor and acceptor images. This processed donor (D) image was divided by the processed acceptor (A) image to get a pseudo color D/A image, using Image calculator module of ImageJ [58]. The pH value was calculated by using the equation (2) formulated from *in vivo* and *in vitro* pH calibration plot.

The pseudo colored pH image was processed to get a K_d image as shown in Fig. 3. K_d of *CalipHluor*$_{Ly}$ is a function of pH and this relation is formulated by the K_d calibration plot *in vivo* and *in vitro* using equation (3). For image processing of pH image to K_d image, background was set to a non-zero value. The K_d image represents the affinity of *CalipHluor*$_{Ly}$ for calcium and thus compensating the calcium image (O/R) with K_d would precisely represent the calcium levels at single endo-lysosomes. The pH dependent K_d compensation is performed according to equation (5), where O/R_{max} and O/R_{min} are calculated by incubating CalipHluor coated beads at 10mM and 1μM respectively. Image calculation were done using image calculator module in ImageJ. This image is multiplied with binary image to bring the background value to zero. The pH corrected K_d image were obtained for various mutants for accurate comparison of calcium levels in lysosomes.

Survival assay

+/mT1 II; cup-5(ok1698)/mT1 [dpy-10(e128)] III nematode strain was used for this assay[43]. Homozygous lethal deletion of *cup-5* gene is balanced by *dpy-10*-marked translocation. Heterozygotes are superficially wildtype [*cup5+/−*], *Dpys* (mT1 homozygotes) are sterile, and *cup5(ok1698)* homozygotes are lethal. *cup5+/−* L4 worms were placed on plates containing RNAi bacterial strains for L4440 *empty vector* (positive control), *mrp-4*, *catp-6*, *catp-5* and *clh-6*. These worms were allowed to grow for 24 h and lay eggs after which the adult worms were removed from the plates. The eggs were allowed to hatch and grow to adult for 3 days. The worm plates were then imaged under Olympus SZX-Zb12 Research Stereomicroscope (Olympus Corporation of the Americas, Center Valley, PA, USA) with a Zeiss Axiocam color CCD camera (Carl Zeiss Microscopy, Thornwood, NY, USA). The

images were analyzed using ImageJ software to count the number of adult worms per plate. Three independent plates were used for each RNAi background.

Lysosomal size recovery assay

arIs37 [myo-3p::ssGFP + dpy-20(+)] I. cup-5(ar465) is transgenic nematode strain which secretes GFP from the body muscle cells and this is endocytosed by coelomocytes which show enlarged GFP labelled vesicles as a result of defective degradation caused by *cup 5* mutation [28]. Similar to the previous assay, *arIs37*; *cup-5(ar465)* L4 worms were placed on plates containing RNAi bacterial strains for *empty vector* (control), *catp-6, catp-5* and *mrp-4* (positive control). The worms lay eggs for 24 hours after which they are removed from the plates. The eggs thus hatch and grow to adulthood after which they were imaged to check for lysosomal size differences. Worms were imaged on a Leica TCS SP5 II STED laser scanning confocal microscope (Leica Microsystems, Inc., Buffalo Grove, IL, USA) equipped with 63X, 1.4 NA, oil immersion objective upon excitation with Argon laser in the Alexa 488 channel. Lysosomal areas were measured using ImageJ. Out 100 lysosomes in *arIs37* worms, 7 lysosomes had an area in range of 7.0–9.5 μm^2. Enlarged lysosomes are defined as those lysosomes whose diameter is ≥ 33% of the diameter of the largest lysosome observed in normal N2 worms. We measured the lysosomal area in *arIs37*; *cup-5(ar465)* worms in various RNAi bacteria containing plates. Lysosomal size recovery data was plotted as percentage of area occupied by large lysosomes to the total lysosomal area (n = 15 cells, > 100 lysosomes).

Bead calibration of *CalipHluor^{mLy}*

Bead calibration was performed using *CalipHluor^{mLy}* coated 0.6μm Monodisperse Silica Microspheres (Cospheric, USA). Briefly, silica microspheres were incubated in a solution of 5μM *CalipHluor^{mLy}* in 20mM Sodium Acetate buffer (pH= 5.1) and 500mM NaCl for 1 h[59,60]. This binding solution was then spun down and the beads were reconstituted in clamping buffer [HEPES (10 mM), MES (10 mM), sodium acetate (10 mM), EGTA (10 mM), KCl (140 mM), NaCl (500 mM) and $MgCl_2$ (1 mM)]. We then varied the amount of [Ca^{2+}] from ~0mM to 10 mM and adjusted the pH to either pH 4.6 or pH 5.1. The beads were incubated in clamping buffer for 30 mins after which there were imaged on a slide on the IX83 inverted microscope in the G, O and R channels to obtain G/R (pH) and O/R (Ca^{2+}) images.

Cell culture methods and maintenance

Human dermal fibroblasts (HDF) were a kind gift from Late Professor Janet Rowley's Lab at the University of Chicago and human fibroblast cells harboring mutations in ATP13A2 (L6025) were a kind gift from Krainc Lab, Northwestern University, Chicago. L6025 is homozygous for 1550C>T. Control and mutant fibroblasts were cultured in Dulbecco's Modified Eagle's Medium (Invitrogen Corporation, USA) containing 10% heat inactivated Fetal Bovine Serum (FBS) (Invitrogen Corporation, USA), 100 U/ml penicillin and 100 μg/mL streptomycin and maintained at 37°C under 5 % CO_2.

Competition experiments in cells

HDF cells were washed with 1× PBS buffer pH 7.4 prior to labeling. Cells were incubated with 10 μM of maleylated BSA (mBSA) or BSA for 15 min and pulsed with media containing 500 nM *CalipHluor*^{mLy} and 10 μM of mBSA or BSA for 1 h to allow internalization by receptor mediated endocytosis, washed 3 times with 1× PBS and then imaged under a wide-field microscope. Whole cell intensities in the Alexa 647 channel was quantified for >30 cells per dish. The mean intensity from three different experiments were normalized with respect to the autofluorescence and presented as the fraction internalized.

Colocalization in cells

We used lysosomes pre-labeled with 10kDa TMR-Dextran (TMR-Dex) to study the trafficking time scales for our probes. TMR Dex was pulsed for 1 h, chased for 16 h in fibroblast cells followed by imaging. Pre-labeled cells were pulsed with 500nM of *CalipHluor*$_{A647Ly}$ and chased for indicated time and imaged. Cross talk and bleed-through were measured and found to be negligible between the TMR channel and Alexa 647 channel. Pearsons correlation coefficient (PCC) measures the pixel-by-pixel covariance in the signal levels of two images. Tools for quantifying PCC are provided in Fuji software. Pearsons correlation coefficient (PCC) measures the pixel-by-pixel covariance in the signal levels of two images. Tools for quantifying PCC are provided in Fuji software.

In cellulo measurements pH and calcium measurements

pH and calcium clamping were carried out using *CalipHluor*^{mLy}. Fibroblast cells were pulsed for 1 h and chased for 2 h with 500nM *CalipHluor*^{mLy}. Cells are then fixed with 200 mL 4% paraformaldehyde (PFA) for 15 min at room temperature, washed three times and retained in 1× PBS. To obtain the intracellular pH and calcium calibration profile, endosomal calcium concentrations were equalized by incubating the previously fixed cells in the appropriate calcium clamping buffer [HEPES (10 mM), MES (10 mM), sodium acetate (10 mM), EGTA (10 mM), KCl (140 mM), NaCl (5 mM) and $MgCl_2$ (1 mM)] by varying amount of free [Ca^{2+}] from 1 μM to 10 mM and adjusted to different pH values. The buffer also contained nigericin (50 μM), monensin (50 μM) and ionomycin (20 μM) and the cells were incubated for 2 h at room temperature.

For realtime pH and calcium measurements, fibroblast cells are pulsed with 500nM of *CalipHluor*^{mLy} for 1 h, chased for 9 h (8 h for L0625 cells) and then washed with 1× PBS and imaged in Hank's Balanced Salt Solution (HBSS). Imaging was carried out on IX83 research inverted microscope (Olympus Corporation of the Americas, Center Valley, PA, USA) using a 100X, 1.42 NA, DIC oil immersion objective (PLAPON, Olympus Corporation of the Americas, Center Valley, PA, USA) and Evolve Delta 512 EMCCD camera (Photometrics, USA).

Data availability

The data that support the plots within this paper and the findings of this study are available from the corresponding author upon reasonable request.

Life Sciences Reporting Summary

Further information on experimental design is available in the Life Sciences Reporting Summary.

Supplementary Material

Refer to Web version on PubMed Central for supplementary material.

Acknowledgements

We thank Professor John Kuriyan and Matthew Zajac for valuable comments. We thank the Integrated Light Microscopy facility at the University of Chicago, the Caenorhabditis Genetic Center (CGC) for strains and Ausubel Lab for Arhinger Library RNAi clones. This work was supported by the University of Chicago Women's Board, Pilot and Feasibility award from an NIDDK center grant P30DK42086 to the University of Chicago Digestive Diseases Research Core Center, MRSEC grant no. DMR-1420709, National Center for Advancing Translational Sciences (NCATS) of the National Institutes of Health (NIH) through Grant Number 1UL1TR002389-01 that funds the Institute for Translational Medicine (ITM), Chicago Biomedical Consortium with support from the Searle Funds at The Chicago Community Trust, C-084 and University of Chicago start-up funds to Y.K. Y.K. is a Brain Research Foundation Fellow.

References

1. Clapham DE Calcium signaling. Cell 131, 1047–1058 (2007). [PubMed: 18083096]
2. Bagur R. & Hajnóczky G. Intracellular ca2+ sensing: its role in calcium homeostasis and signaling. Mol. Cell 66, 780–788 (2017). [PubMed: 28622523]
3. Yang J, Zhao Z, Gu M, Feng X. & Xu H. Release and uptake mechanisms of vesicular Ca2+ stores. Protein Cell (2018). doi:10.1007/s13238-018-0523-x
4. Parenti G, Andria G. & Ballabio A. Lysosomal storage diseases: from pathophysiology to therapy. Annu. Rev. Med 66, 471–486 (2015). [PubMed: 25587658]
5. Plotegher N. & Duchen MR Crosstalk between Lysosomes and Mitochondria in Parkinson's Disease. Front. Cell Dev. Biol 5, 110 (2017). [PubMed: 29312935]
6. Xu H, Martinoia E. & Szabo I. Organellar channels and transporters. Cell Calcium 58, 1–10 (2015). [PubMed: 25795199]
7. Calcraft PJ et al. NAADP mobilizes calcium from acidic organelles through two-pore channels. Nature 459, 596–600 (2009). [PubMed: 19387438]
8. Huang P. et al. P2X4 forms functional ATP-activated cation channels on lysosomal membranes regulated by luminal pH. J. Biol. Chem 289, 17658–17667 (2014). [PubMed: 24817123]
9. Kiselyov K. et al. TRPML: transporters of metals in lysosomes essential for cell survival? Cell Calcium 50, 288–294 (2011). [PubMed: 21621258]
10. Lloyd-Evans E. On the move, lysosomal CAX drives Ca2+ transport and motility. J. Cell Biol 212, 755–757 (2016). [PubMed: 27022089]
11. Melchionda M, Pittman JK, Mayor R. & Patel S. Ca2+/H+ exchange by acidic organelles regulates cell migration in vivo. J. Cell Biol 212, 803–813 (2016). [PubMed: 27002171]
12. Morgan AJ, Davis LC & Galione A. Imaging approaches to measuring lysosomal calcium. Methods Cell Biol. 126, 159–195 (2015). [PubMed: 25665446]
13. Christensen KA, Myers JT & Swanson JA pH-dependent regulation of lysosomal calcium in macrophages. J. Cell Sci 115, 599–607 (2002). [PubMed: 11861766]
14. Lloyd-Evans E. et al. Niemann-Pick disease type C1 is a sphingosine storage disease that causes deregulation of lysosomal calcium. Nat. Med 14, 1247–1255 (2008). [PubMed: 18953351]
15. Garrity AG et al. The endoplasmic reticulum, not the pH gradient, drives calcium refilling of lysosomes. Elife 5, (2016).
16. Sherwood MW et al. Activation of trypsinogen in large endocytic vacuoles of pancreatic acinar cells. Proc. Natl. Acad. Sci. USA 104, 5674–5679 (2007). [PubMed: 17363470]

17. Gerasimenko JV, Tepikin AV, Petersen OH & Gerasimenko OV Calcium uptake via endocytosis with rapid release from acidifying endosomes. Curr. Biol 8, 1335–1338 (1998). [PubMed: 9843688]
18. Johnson DE, Ostrowski P, Jaumouillé V. & Grinstein S. The position of lysosomes within the cell determines their luminal pH. J. Cell Biol 212, 677–692 (2016). [PubMed: 26975849]
19. Chakraborty K, Veetil AT, Jaffrey SR & Krishnan Y. Nucleic Acid-Based Nanodevices in Biological Imaging. Annu. Rev. Biochem 85, 349–373 (2016). [PubMed: 27294440]
20. Modi S. et al. A DNA nanomachine that maps spatial and temporal pH changes inside living cells. Nat. Nanotechnol 4, 325–330 (2009). [PubMed: 19421220]
21. Surana S, Bhat JM, Koushika SP & Krishnan Y. An autonomous DNA nanomachine maps spatiotemporal pH changes in a multicellular living organism. Nat. Commun 2, 340 (2011). [PubMed: 21654640]
22. Saha S, Prakash V, Halder S, Chakraborty K. & Krishnan Y. A pH-independent DNA nanodevice for quantifying chloride transport in organelles of living cells. Nat. Nanotechnol 10, 645–651 (2015). [PubMed: 26098226]
23. Modi S, Nizak C, Surana S, Halder S. & Krishnan Y. Two DNA nanomachines map pH changes along intersecting endocytic pathways inside the same cell. Nat. Nanotechnol 8, 459–467 (2013). [PubMed: 23708428]
24. Chakraborty K, Leung K. & Krishnan Y. High lumenal chloride in the lysosome is critical for lysosome function. Elife 6, e28862 (2017). [PubMed: 28742019]
25. Toyoshima C. & Inesi G. Structural basis of ion pumping by Ca2+-ATPase of the sarcoplasmic reticulum. Annu. Rev. Biochem 73, 269–292 (2004). [PubMed: 15189143]
26. Schmidt K, Wolfe DM, Stiller B. & Pearce DA Cd2+, Mn2+, Ni2+ and Se2+ toxicity to Saccharomyces cerevisiae lacking YPK9p the orthologue of human ATP13A2. Biochem. Biophys. Res. Commun 383, 198–202 (2009). [PubMed: 19345671]
27. Ramonet D. et al. PARK9-associated ATP13A2 localizes to intracellular acidic vesicles and regulates cation homeostasis and neuronal integrity. Hum. Mol. Genet 21, 1725–1743 (2012). [PubMed: 22186024]
28. Fares H. & Greenwald I. Regulation of endocytosis by CUP-5, the Caenorhabditis elegans mucolipin-1 homolog. Nat. Genet 28, 64–68 (2001). [PubMed: 11326278]
29. Salgado EN, Garcia Rodriguez B, Narayanaswamy N, Krishnan Y. & Harrison SC Visualization of Ca2+ loss from rotavirus during cell entry. J. Virol (2018). doi:10.1128/JVI.01327-18
30. Jewett JC, Sletten EM & Bertozzi CR Rapid Cu-free click chemistry with readily synthesized biarylazacyclooctynones. J. Am. Chem. Soc 132, 3688–3690 (2010). [PubMed: 20187640]
31. Huotari J. & Helenius A. Endosome maturation. EMBO J. 30, 3481–3500 (2011). [PubMed: 21878991]
32. Hu Y-B, Dammer EB, Ren R-J & Wang G. The endosomal-lysosomal system: from acidification and cargo sorting to neurodegeneration. Transl Neurodegener 4, 18 (2015). [PubMed: 26448863]
33. Vandecaetsbeek I, Vangheluwe P, Raeymaekers L, Wuytack F. & Vanoevelen J. The Ca2+ pumps of the endoplasmic reticulum and Golgi apparatus. Cold Spring Harb. Perspect. Biol 3, (2011).
34. Tharkeshwar AK et al. A novel approach to analyze lysosomal dysfunctions through subcellular proteomics and lipidomics: the case of NPC1 deficiency. Sci. Rep 7, 41408 (2017). [PubMed: 28134274]
35. Chapel A. et al. An extended proteome map of the lysosomal membrane reveals novel potential transporters. Mol. Cell Proteomics 12, 1572–1588 (2013). [PubMed: 23436907]
36. Lübke T, Lobel P. & Sleat DE Proteomics of the lysosome. Biochim. Biophys. Acta 1793, 625–635 (2009). [PubMed: 18977398]
37. Brozzi A, Urbanelli L, Germain PL, Magini A. & Emiliani C. hLGDB: a database of human lysosomal genes and their regulation. Database (Oxford) 2013, bat024 (2013). [PubMed: 23584836]
38. Schröder BA, Wrocklage C, Hasilik A. & Saftig P. The proteome of lysosomes. Proteomics 10, 4053–4076 (2010). [PubMed: 20957757]

39. Cao Q, Yang Y, Zhong XZ & Dong X-P The lysosomal Ca2+ release channel TRPML1 regulates lysosome size by activating calmodulin. J. Biol. Chem 292, 8424–8435 (2017). [PubMed: 28360104]
40. Sahoo N. et al. Gastric Acid Secretion from Parietal Cells Is Mediated by a Ca2+ Efflux Channel in the Tubulovesicle. Dev. Cell 41, 262–273.e6 (2017). [PubMed: 28486130]
41. Bargal R. et al. Identification of the gene causing mucolipidosis type IV. Nat. Genet 26, 118–123 (2000). [PubMed: 10973263]
42. Schaheen L, Dang H. & Fares H. Basis of lethality in C. elegans lacking CUP-5, the Mucolipidosis Type IV orthologue. Dev. Biol 293, 382–391 (2006). [PubMed: 16530747]
43. elegans C. Deletion Mutant Consortium. large-scale screening for targeted knockouts in the Caenorhabditis elegans genome. G3 (Bethesda) 2, 1415–1425 (2012). [PubMed: 23173093]
44. Schaheen L, Patton G. & Fares H. Suppression of the cup-5 mucolipidosis type IV-related lysosomal dysfunction by the inactivation of an ABC transporter in C. elegans. Development 133, 3939–3948 (2006). [PubMed: 16943270]
45. Fares H. & Greenwald I. Genetic analysis of endocytosis in Caenorhabditis elegans: coelomocyte uptake defective mutants. Genetics 159, 133–145 (2001). [PubMed: 11560892]
46. van Veen S. et al. Cellular function and pathological role of ATP13A2 and related P-type transport ATPases in Parkinson's disease and other neurological disorders. Front. Mol. Neurosci 7, 48 (2014). [PubMed: 24904274]
47. Schöndorf DC et al. iPSC-derived neurons from GBA1-associated Parkinson's disease patients show autophagic defects and impaired calcium homeostasis. Nat. Commun 5, 4028 (2014). [PubMed: 24905578]
48. Usenovic M, Tresse E, Mazzulli JR, Taylor JP & Krainc D. Deficiency of ATP13A2 leads to lysosomal dysfunction, α-synuclein accumulation, and neurotoxicity. J. Neurosci 32, 4240–4246 (2012). [PubMed: 22442086]
49. Bras J, Verloes A, Schneider SA, Mole SE & Guerreiro RJ Mutation of the parkinsonism gene ATP13A2 causes neuronal ceroid-lipofuscinosis. Hum. Mol. Genet 21, 2646–2650 (2012). [PubMed: 22388936]
50. Estrada-Cuzcano A. et al. Loss-of-function mutations in the ATP13A2/PARK9 gene cause complicated hereditary spastic paraplegia (SPG78). Brain 140, 287–305 (2017). [PubMed: 28137957]

References

51. Grynkiewicz G, Poenie M. & Tsien RY A new generation of Ca2+ indicators with greatly improved fluorescence properties. J. Biol. Chem 260, 3440–3450 (1985). [PubMed: 3838314]
52. Collot M. et al. CaRuby-Nano: a novel high affinity calcium probe for dual color imaging. Elife 4, (2015).
53. Moore D. & Dowhan D. Purification and concentration of DNA from aqueous solutions. Curr. Protoc. Mol. Biol Chapter 2, Unit 2.1A (2002).
54. Brenner S. The genetics of Caenorhabditis elegans. Genetics 77, 71–94 (1974). [PubMed: 4366476]
55. Kamath RS & Ahringer J. Genome-wide RNAi screening in Caenorhabditis elegans. Methods 30, 313–321 (2003). [PubMed: 12828945]
56. Evangelidis GD & Psarakis EZ Parametric image alignment using enhanced correlation coefficient maximization. IEEE Trans. Pattern Anal. Mach. Intell 30, 1858–1865 (2008). [PubMed: 18703836]
57. Sauvola J. & Pietikäinen M. Adaptive document image binarization. Pattern Recognit 33, 225–236 (2000).
58. Schindelin J. et al. Fiji: an open-source platform for biological-image analysis. Nat. Methods 9, 676–682 (2012). [PubMed: 22743772]
59. Engelstein M. et al. An efficient, automatable template preparation for high throughput sequencing. Microb. Comp. Genomics 3, 237–241 (1998). [PubMed: 10027192]

60. Vandeventer PE et al. Multiphasic DNA adsorption to silica surfaces under varying buffer, pH, and ionic strength conditions. J. Phys. Chem. B 116, 5661–5670 (2012). [PubMed: 22537288]

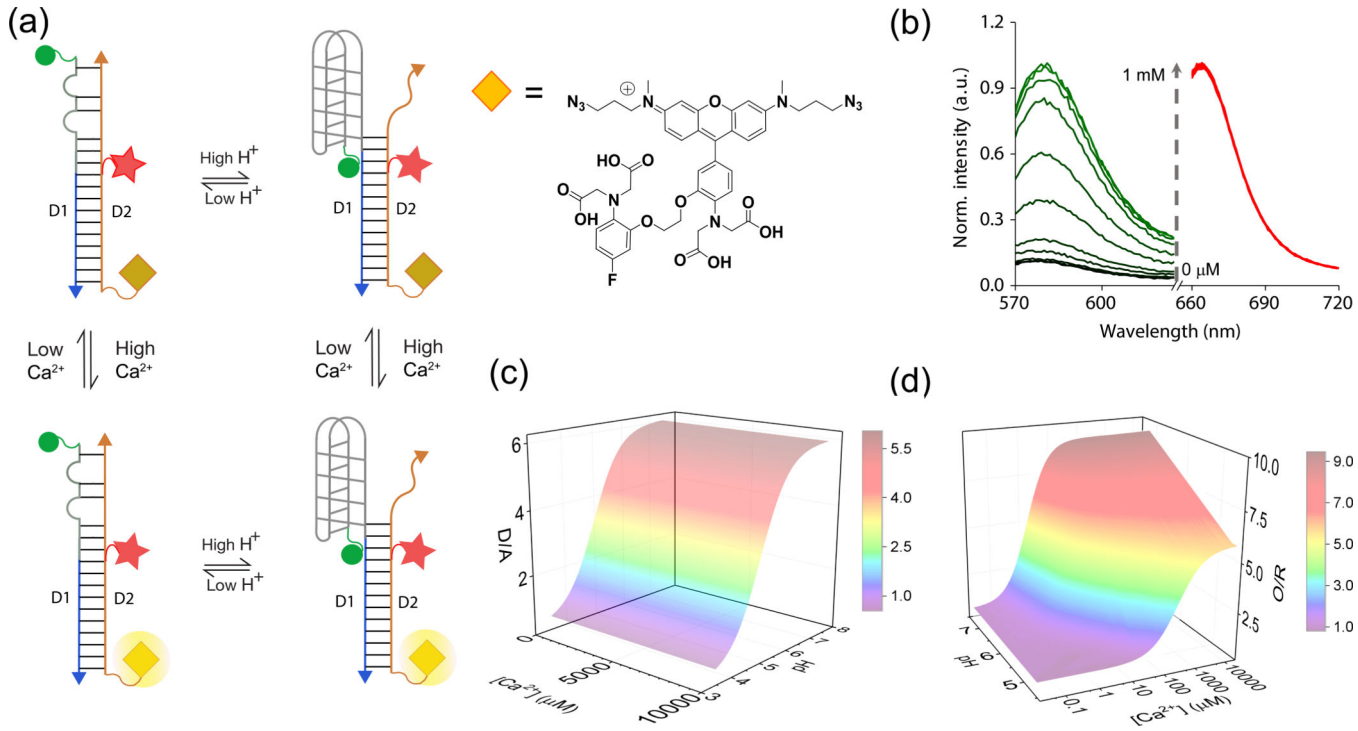

Figure-1: Design and characterization of *CalipHluor$_{Ly}$*.

(a) Working principle of ***CalipHluor$_{Ly}$***. pH-induced FRET between Alexa488 (donor, D, green sphere) and Alexa647 (acceptor, A, red star) reports on pH ratiometrically. A Ca^{2+} sensitive dye (Rhod-5F, yellow diamond, λ_{ex}=560 nm) and Alexa647 (λ_{ex}=650 nm) report Ca^{2+} ratiometrically by direct excitation. (b) Fluorescence emission spectra of ***CalipHluor$_{Ly}$*** corresponding to Rhod-5F (green, O) and Alexa647 (red, R) with increasing [Ca^{2+}] at pH = 7.2. (c) 3D-surface plot of donor to acceptor ratio (D/A) or pH response of ***CalipHluor$_{Ly}$*** as a function of pH and [Ca^{2+}]. (d) 3D-surface plot of the Rhod-5F to Alexa647 ratio (O/R) or Ca^{2+} response of ***CalipHluor$_{Ly}$*** as a function of pH and [Ca^{2+}].

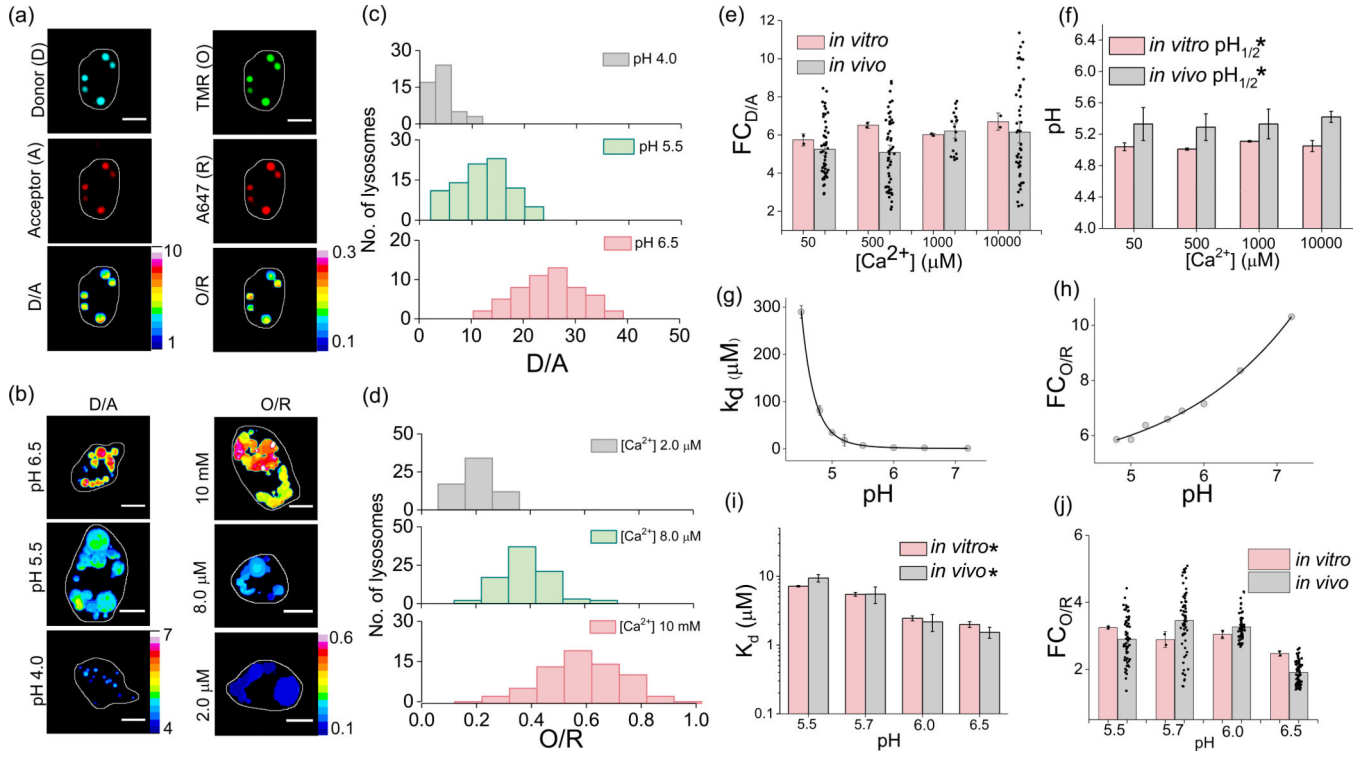

Figure-2: *In vivo* sensing characteristics of *CalipHluor$_{Ly}$*.

(a) Representative ***CalipHluor$_{Ly}$*** labelled coelomocytes imaged in the donor (D,**i**), acceptor (A,**ii**), Rhod-5F (O, **iii**) and Alexa647 (R, **iv**) channels. D/A (**v**) and O/R (**vi**) are the corresponding pixel-wise pseudocolor images. (b) Representative pseudo colored D/A and O/R maps of coelomocytes clamped at indicated pH and free [Ca^{2+}] (c) Distribution of D/A ratios of ≥ 50 endosomes clamped at the indicated pH (n = 10 cells). (d) Distribution of O/R ratios of ≥ 50 endosomes clamped at different indicated free [Ca^{2+}] (n = 10 cells). Comparison of (e) fold change of D/A ratios from pH 4 to 6.5 and; (f) $pH_{1/2}$ from pH 4 to 6.5 of ***CalipHluor$_{Ly}$*** at different [Ca^{2+}] obtained *in vitro* (peach) and *in vivo* (gray). ***CalipHluor$_{Ly}$*** (g) Dissociation constant K_d (μM) and (h) fold change of O/R as a function of pH. Comparison of (i) fold change in O/R ratio from 1 μM to 10 mM [Ca^{2+}] and (j) Dissociation constant K_d (μM) of ***CalipHluor$_{Ly}$*** at the indicated pH obtained *in vitro* (peach) and *in vivo* (gray). Scale bars, 5 μm. Data represent mean ± s.e.m. * Error is obtained from the non-exponential fit. Experiments were repeated thrice independently with similar results.

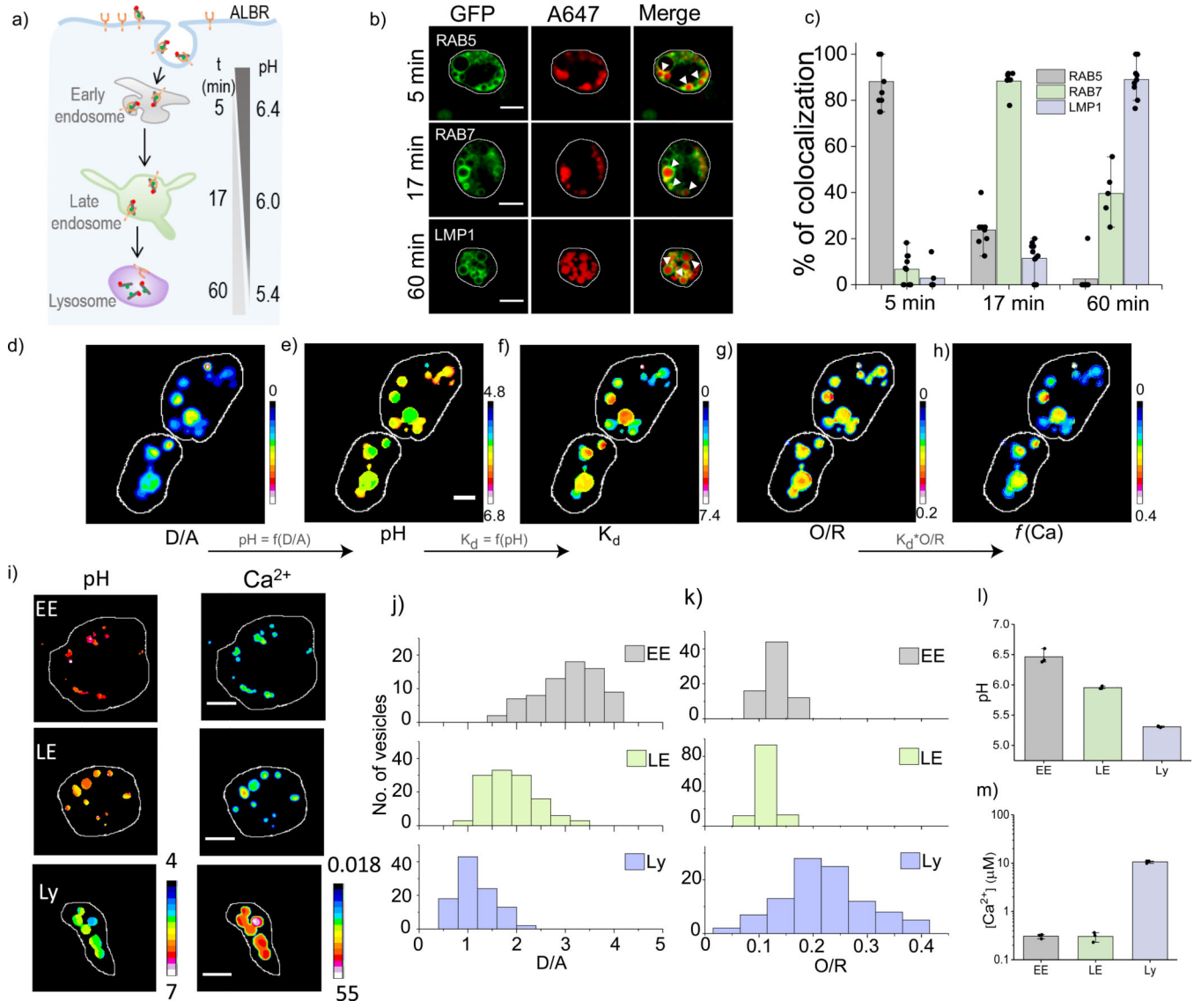

Figure-3: pH and [Ca^{2+}] maps accompanying endosomal maturation.

(**a**) ***CalipHluor*** marks the indicated organelles in coelomocytes time dependently, by scavenger receptor mediated endocytosis. (**b**) Colocalization of ***CalipHluor*** and GFP-tagged markers of endocytic organelles at indicated time points post-injection in nematodes. (**c**) Quantification of colocalization in (**b**) (n = 10 cells, ≥ 50 endosomes) Pseudo color images of ***CalipHluor***$_{Ly}$ labelled lysosomes where the D/A map (**d**) is converted to the corresponding pH map (**e**), the pH map is converted into a K_d map (**f**) where the value of K_d is encoded pixelwise according to the pH at that pixel; the K_d map (**f**) is multiplied by the O/R map (**g**) to yield the Ca^{2+} map (**h**). (**i**) Representative pseudocolor pH and Ca^{2+} maps of early endosomes (EE), late endosomes (LE) and lysosomes (Ly) labelled with ***CalipHluor*** *and* ***CalipHluor***$_{Ly}$. (**j-l**) Distributions of D/A and O/R ratios of EE, LE and Ly from n = 15 cells, 50 endosomes. (h) Mean endosomal pH of EE, LE and Ly. (i) Mean endosomal [Ca^{2+}] in EE, LE and Ly data represent the mean ± s.e.m. Experiments were repeated thrice independently with similar results.

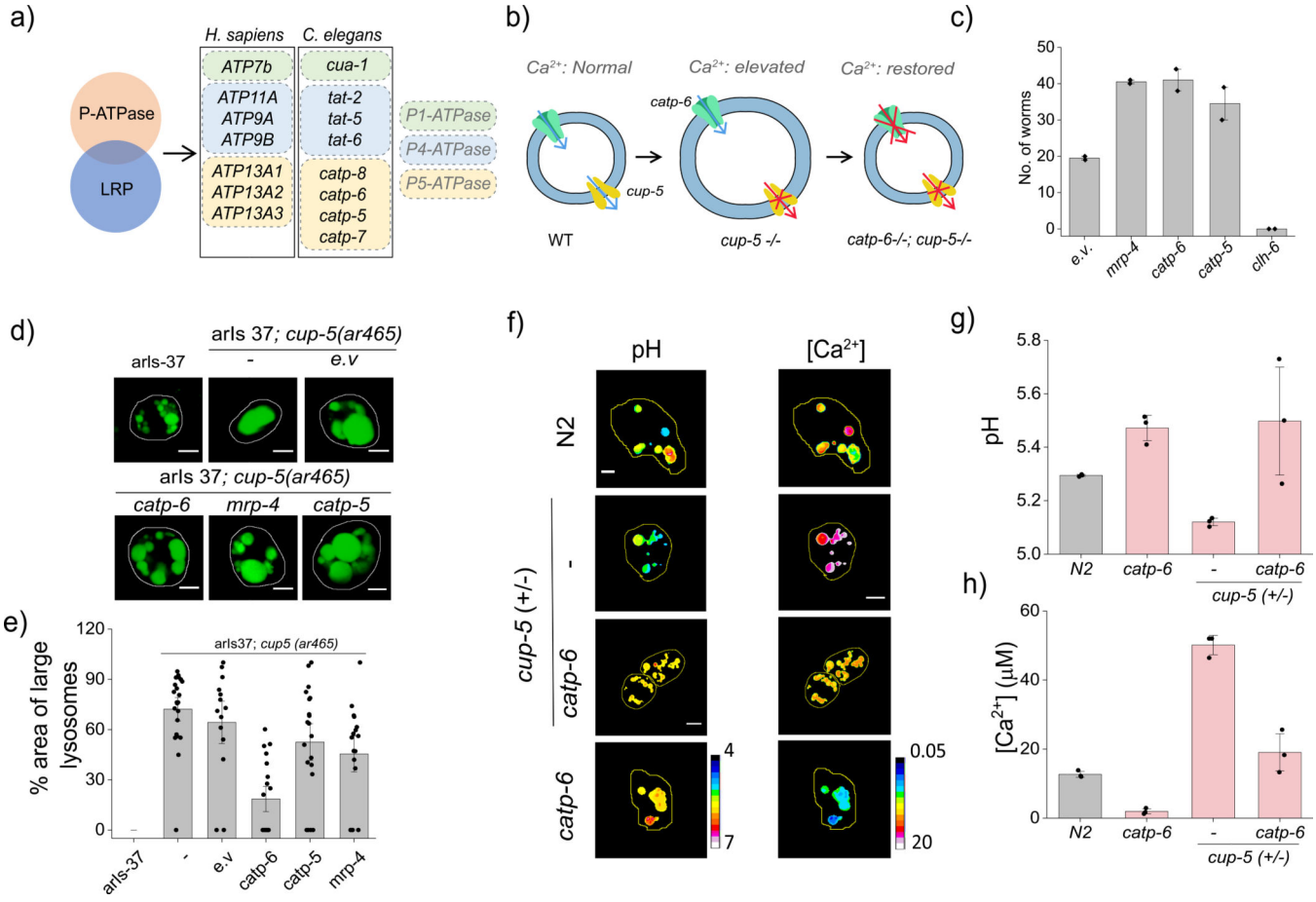

Figure-4: *Catp-6* facilitates lysosomal Ca^{2+} accumulation:

(a) P-type ATPases in human lysosomes obtained from the human Lysosome Gene Database (hLGDB). (b) Functional connectivity between *catp-6* and *cup-5*. (c) Number of adult *cup-5 +/−* progeny where the indicated proteins are knocked down by RNAi. Data represents mean ± s.e.m. of three independent trials. (d) Representative fluorescence images of *arIs37[myo-3p::ssGFP + dpy-20 (+)]I* and *arIs37; cup5(ar465)* upon RNAi knockdown of the indicated proteins. (e) Percentage area occupied by enlarged lysosomes in the indicated genetic background. (n = 15 cells, ≥ 100 lysosomes). (f) pH and Ca^{2+} maps in ***CalipHluor*$_{Ly}$**-labeled lysosomes in coelomocytes in indicated genetic backgrounds (g) Mean lysosomal pH and (h) mean lysosomal [Ca^{2+}] in the indicated genetic backgrounds. Data represent the mean ± s.e.m. Scale bar 5 μm. Data represent mean ± s.e.m. Experiments were repeated thrice independently with similar results.

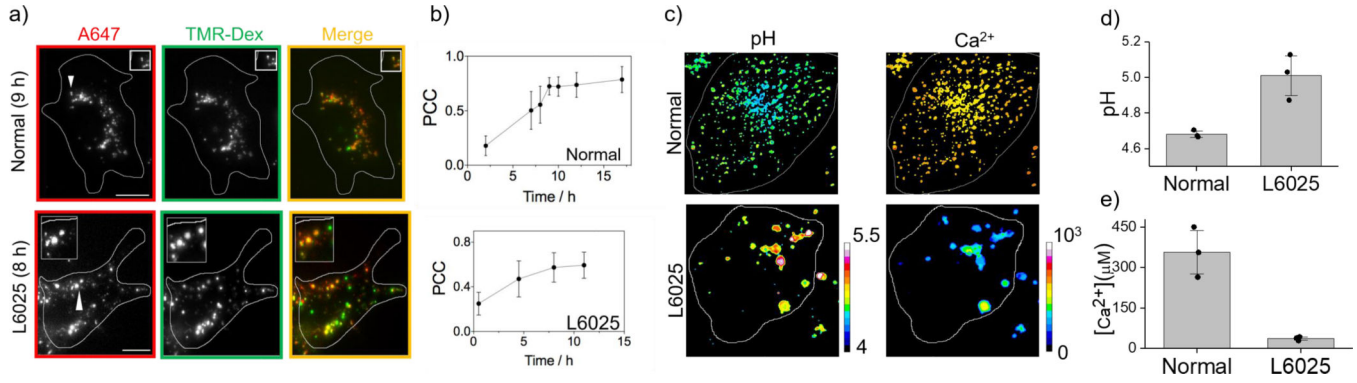

Figure-5: *CalipHuor*^{mLy} maps lysosomal Ca^{2+} in human cells:

a) Representative images of lysosomes in fibroblast cells from normal individuals and Kufor Rakeb syndrome patients (L6025S) labelled with TMR dextran (TMR; green) and ***CalipHluor***^{mLy} (Alexa647, red). b) Pearson's correlation coefficient (PCC) of colocalization between ***CalipHluor***^{mLy} and lysosomes as a function of time (n = 20 cells). c) Pseudocolor pH and Ca^{2+} maps of lysosomes in normal and L6025 fibroblasts (d) Mean lysosomal pH and (e) mean lysosomal [Ca^{2+}] in normal and L6025 fibroblasts. (n = 5 cells; 50 endosomes) Scale bar: 10 μm. Data represent mean ± s.e.m. Experiments were repeated thrice independently with similar results.